PHYSICS OF EARTH, ATMOSPHERE, AND HYDROSPHERE

Numerical Modeling of the Effect of Inflow Water Mineralization in the Dynamics of the Autumnal Thermal Bar in Kamloops Lake

B. O. Tsydenov*

*Computational Geophysics Laboratory, Faculty of Mechanics and Mathematics,
Tomsk State University, Tomsk, 634050 Russia*
*e-mail: tsydenov@math.tsu.ru

Abstract—The results of numerical modeling of hydrodynamic processes that occur during the period of existence of an autumnal thermal bar in Kamloops Lake, Canada are presented. These results were obtained using a nonhydrostatic 2.5D model in the Boussinesq approximation with allowance for the diurnal variability of radiative and turbulent heat fluxes at the surface of the lake. A series of numerical experiments with various values of water mineralization in the Thompson River have been performed. The calculations show that the mineralization of inflow river waters has a significant effect on the dynamics of horizontal movements of the thermal front and on the pattern of circulation flows induced by the thermal bar during the period of lake cooling.

INTRODUCTION

In lakes of moderate latitudes, the phenomenon of a thermal bar, which is a narrow zone of water sinking, occurs twice a year: in spring and autumn. Such a phenomenon was first discovered in Lake Geneva in 1880 by F.A. Forel, a Swiss limnologist [1]. A thermal bar is formed in the periods of spring heating and autumn cooling of a water body. Due to mixing of waters with different temperatures and salinity characteristics, the densest water masses sink, thus forming a frontal interface. In the classical sense, the water temperature inside the front of a thermal bar is 4°C [1, 2]. A thermal bar prevents horizontal water exchange, which greatly affects the life of plankton communities, the water quality, and the lake ecosystem as a whole.

Different mathematical models exist to study the effect of a thermal bar in a freshwater lake [3–7]. However, these models do not take account of a very important factor of the formation and evolution of a thermal bar, namely, the real diurnal variability of radiative and turbulent heat fluxes at the surface of a lake (as a rule, a constant heat flux is prescribed in a model that corresponds to the monthly average solar radiation). In addition, whereas a great amount of data on features of a spring thermal bar have been obtained by numerical experiments [3–11], knowledge of hydrophysical processes that occur during the

period of existence of an autumnal thermal bar is very limited.

It is known that the water density depends on not only the temperature but also the salinity. Therefore, studying the dependence of hydrodynamic processes on water mineralization is of particular interest. The purpose of this work is to numerically study the effect of inflow water mineralization on the evolution of an autumnal thermal bar using Kamloops Lake as an example. For this, we use a nonhydrostatic 2.5D model [12] with allowance for the diurnal variability of the state of the atmosphere and real morphometric conditions of the lake.

1. MATHEMATICAL MODEL

1.1. Basic Equations of the Model

The nonhydrostatic 2.5D model used to reproduce the lake hydrodynamics and study the salinity effects of river waters during the period of existence of an autumnal thermal bar in a large water body includes the following equations:

■ the equation of the salinity (mineralization) balance

$$\frac{\partial S}{\partial t} + \frac{\partial uS}{\partial x} + \frac{\partial wS}{\partial z} = \frac{\partial}{\partial x}\left(D_x \frac{\partial S}{\partial x}\right) + \frac{\partial}{\partial z}\left(D_z \frac{\partial S}{\partial z}\right); \quad (1)$$

- the equation of energy

$$\frac{\partial T}{\partial t} + \frac{\partial uT}{\partial x} + \frac{\partial wT}{\partial z}$$
$$= \frac{\partial}{\partial x}\left(D_x \frac{\partial T}{\partial x}\right) + \frac{\partial}{\partial z}\left(D_z \frac{\partial T}{\partial z}\right) + \frac{1}{\rho_0 c_p}\frac{\partial H_{\text{sol}}}{\partial z}; \quad (2)$$

- the momentum equation

$$\frac{\partial u}{\partial t} + \frac{\partial u^2}{\partial x} + \frac{\partial uw}{\partial z} = -\frac{1}{\rho_0}\frac{\partial p}{\partial x} + \frac{\partial}{\partial x}\left(K_x \frac{\partial u}{\partial x}\right)$$
$$+ \frac{\partial}{\partial z}\left(K_z \frac{\partial u}{\partial z}\right) + 2\Omega_z v - 2\Omega_y w, \quad (3)$$

$$\frac{\partial v}{\partial t} + \frac{\partial uv}{\partial x} + \frac{\partial wv}{\partial z} = \frac{\partial}{\partial x}\left(K_x \frac{\partial v}{\partial x}\right)$$
$$+ \frac{\partial}{\partial z}\left(K_z \frac{\partial v}{\partial z}\right) + 2\Omega_x w - 2\Omega_z u, \quad (4)$$

$$\frac{\partial w}{\partial t} + \frac{\partial uw}{\partial x} + \frac{\partial w^2}{\partial z} = -\frac{1}{\rho_0}\frac{\partial p}{\partial z} + \frac{\partial}{\partial x}\left(K_x \frac{\partial w}{\partial x}\right)$$
$$+ \frac{\partial}{\partial z}\left(K_z \frac{\partial w}{\partial z}\right) - \frac{g\rho}{\rho_0} + 2\Omega_y u - 2\Omega_x v; \quad (5)$$

- the continuity equation

$$\frac{\partial u}{\partial x} + \frac{\partial w}{\partial z} = 0. \quad (6)$$

Here, S is salinity; T is temperature: u and v are the horizontal velocity components (along the x and y axes, respectively); w is the vertical velocity component (along the z axis); Ω_x, Ω_y, and Ω_z are the components of the vector of the angular velocity of the Earth's rotation; $K_x(D_x)$ and $K_z(D_z)$ are the coefficients of turbulent viscosity (diffusion) along the corresponding directions; g is the acceleration of gravity; c_p is specific heat; p is pressure; and ρ_0 is the water density at the standard atmospheric pressure, temperature T_L, and salinity S_L.

The absorption of solar (short-wave) radiation H_{sol} is calculated according to the Beer–Lambert–Bouguer law

$$H_{\text{sol}} = H_{S\text{sol},0}(1 - r_s)\exp(-\epsilon_{\text{abs}}d), \quad (7)$$

where $r_s \approx 0.2$ is the water-reflection coefficient; $\epsilon_{\text{abs}} \approx 0.3\ \text{m}^{-1}$ is the coefficient of solar radiation absorption in water; and $d = |L_z - z|$ is the depth, m. The short-wave radiation influx $H_{S\text{sol},0}$ at the lake surface is determined by the relation

$$H_{S\text{sol},0} = \begin{cases} S_0(a_g - a_w)\cos\zeta[a(C) + b(C)\ln(\cos\zeta)], \\ (\cos\zeta) > 0; \\ 0, \quad (\cos\zeta) \le 0, \end{cases} \quad (8)$$

where $S_0 = 1367\ \text{W/m}^2$ is the solar constant; $a(C)$ and $b(C)$ are empirical coefficients that depend on the extent of coverage of the sky by clouds C [13]; ζ is the solar zenith angle; the empirical functions a_g and

a_w are the molecular scattering and absorption of permanent gases, respectively.

The coefficients of the momentum and heat diffusive transport intensity are determined based on the $k-\omega$ turbulence model [14] and algebraic relationships [15].

To calculate the water density, we use the Chen–Millero equation [16]

$$\rho(S, T, p) = \frac{\rho^0}{1 - \dfrac{p}{K}}. \quad (9)$$

Here, ρ_0 is calculated by the formula

$$\rho^0 = 999.8395 + 6.7914 \times 10^{-2}T_C - 9.0894 \times 10^{-3}T_C^2$$
$$+ 1.0171 \times 10^{-4}T_C^3 - 1.2846 \times 10^{-6}T_C^4$$
$$+ 1.1592 \times 10^{-8}T_C^5 - 5.0125 \times 10^{-11}T_C^6$$
$$+ (0.8181 - 3.85 \times 10^{-3}T_C + 4.96 \times 10^{-5}T_C^2)S; \quad (10)$$

and the volumetric elastic modulus K is determined as

$$K = 19625.17 + 148.113T_C - 2.293T_C^2$$
$$+ 1.256 \times 10^{-2}T_C^3 - 4.18 \times 10^{-5}T_C^4$$
$$+ (3.2726 - 2.147 \times 10^{-4}T_C + 1.128 \times 10^{-4}T_C^2)p$$
$$+ (53.238 - 0.313T_C + 5.728 \times 10^{-3}p)S, \quad (11)$$

where T_C is the water temperature, °C.

The temperature of the maximum density is calculated by the formula [16]

$$T_{\text{md}} = 3.9839 - 1.9911 \times 10^{-2}p - 5.822 \times 10^{-6}p^2$$
$$- (0.2219 + 1.106 \times 10^{-4}p)S. \quad (12)$$

The method for numerically solving the model equations was described in [17, 18].

1.2. Initial and Boundary Conditions

Initial conditions (at $t = 0$) for the equations of the model are prescribed in the form

$$u = 0, \quad v = 0, \quad w = 0, \quad S = S_L, \quad T = T_L, \quad (13)$$

where S_L and T_L are the salinity and temperature of the water in the lake, respectively.

The boundary conditions for the equations have the form

(a) at the water–air interface

$$K_z \frac{\partial u}{\partial z} = \frac{\tau_{\text{surf}}^u}{\rho_0}, \quad K_z \frac{\partial v}{\partial z} = \frac{\tau_{\text{surf}}^v}{\rho_0}, \quad w = 0,$$
$$\frac{\partial S}{\partial z} = 0, \quad D_z \frac{\partial T}{\partial z} = \frac{H_{\text{net}}}{\rho_0 c_p}, \quad (14)$$

where τ_{surf}^u and τ_{surf}^v are the components of the wind shear stress and H_{net} is the heat flux including the

components of long-wave radiation (H_{lw}), latent heat (H_L), and sensible heat (H_S), which are parametrized according to calculation formulas of model 3 in [19]:

$$H_{lw} = \epsilon_w \epsilon_a \sigma (1 + 0.17 C^2) T_A^4 - \epsilon_w \sigma T^4, \qquad (15)$$

where ϵ_w and ϵ_a are the coefficients of water and atmosphere radiation, σ is the Stefan−Boltzmann constant, T_A is the air temperature, and T is the water temperature;

$$H_L = f_u(e_A - e_w), \quad f_u = 6.9 + 0.345 U^2,$$
$$e_w = 6.112 \exp\left(\frac{17.67(T_A - 273.15)}{T_A - 29.65} \right), \qquad (16)$$

where e_A is the water-vapor pressure in the atmosphere, e_w is the saturated water vapor pressure near the underlying surface, f_u is the mass transfer coefficient, and U is the wind velocity;

$$H_S = 0.62 f_u(T_A - T); \qquad (17)$$

(b) on the solid boundaries (at the bottom)

$$u = 0, \quad v = 0, \quad w = 0,$$
$$\frac{\partial S}{\partial n} = 0, \quad D_z \frac{\partial T}{\partial n} = -\frac{H_{geo}}{\rho_0 c_p}, \qquad (18)$$

where H_{geo} is the geothermal heat and n is the direction of the outer normal to the domain;

(c) at the river−lake interface

$$u = u_R, \quad v = 0, \quad w = 0,$$
$$S = S_R, \quad T = T_R, \qquad (19)$$

where u_R is the inflow velocity at the river mouth, while S_R and T_R are the salinity and temperature of river waters, respectively;

(d) on the open boundary, we prescribe radiation-type conditions [20] and simple gradient conditions

$$\frac{\partial \phi}{\partial t} + c_\phi \frac{\partial \phi}{\partial x} = 0 \ (\phi = u, v, S, T), \quad \frac{\partial w}{\partial x} = 0. \qquad (20)$$

2. THE OBJECT OF RESEARCH AND PROBLEM PARAMETERS

We consider a vertical section of Kamloops Lake, which is located in southwestern Canada (the province of British Columbia) at a distance of 340 km to the northeast of Vancouver between lat. 50°26′–50°45′ N and long. 120°03′–120°32 W along the Thompson River and has an elongated shape (Fig. 1a). The calculation domain has a length of 10 km and a depth of 138 m (Fig. 1b). The x axis is directed along the current of the Thompson River; the origin of the coordinates coincides with the river mouth (Fig. 1a).

The initial water temperature in the lake has a vertically nonhomogeneous distribution

$$T_L(z) = 0.00004 d^2 - 0.0156 d + 279.6, \qquad (21)$$
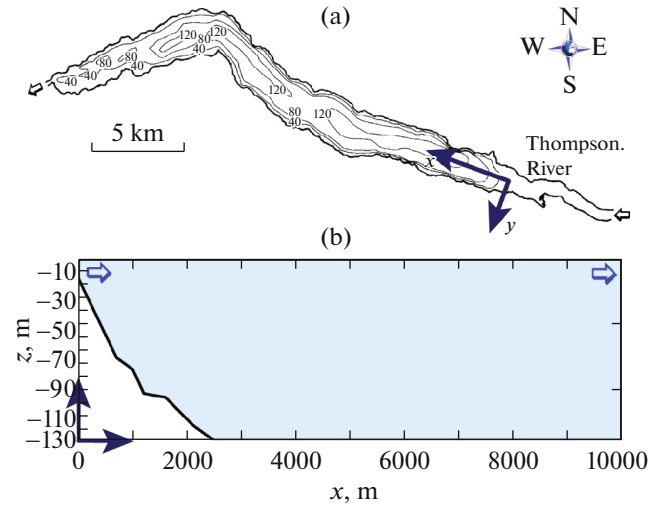
Fig. 1. Kamloops Lake: (a) bathymetry and (b) calculation domain (longitudinal section).

which corresponds to the thermal regime of this water body in autumn periods [21]. According to measurement data of hydrographic stations, the temperature of inflow river waters varies within the range from 2.8 to 0.35°C [21]. The velocity of the Thompson River at the river−lake interface is 3×10^{-3} m/s; the water mineralization in the lake is 0.1 g/kg [22]. The calculation domain (Fig. 1b) is covered by a uniform orthogonal grid with step sizes $h_x = 25$ m and $h_z = 3$ m. The size of the time step is 60 s.

The data on air temperature, relative humidity, atmospheric pressure, and cloudiness are taken from the weather archives of the meteorological station of the city of Kamloops for the period from December 1 through December 30, 2015 (http://climate.weather.gc.ca). To evaluate the extent to which the mineralization of inflow river waters affects the evolution of the thermal bar, we equate the values of H_{geo}, τ^u_{surf}, and τ^v_{surf} to zero in numerical experiments.

3. MODELING RESULTS

3.1. Heat Fluxes at the Lake Surface

Based on the available data of meteorological observations, we calculated the values of the fluxes of short-wave and long-wave radiation and of the latent and sensible heat (Fig. 2). The calculations show that the short-wave radiation flux in December 2015 did not exceed 187.1 W/m². The fluxes of long-wave radiation and latent heat lead to lake cooling and varied within the ranges from −26.3 to −171.2 W/m² and from −1.6 to −81.6 W/m², respectively. Due to increasing air temperature, the sensible heat flux attained positive values in the first decade of the month and was negative in the second and third decades, thus contributing to lake cooling. The range
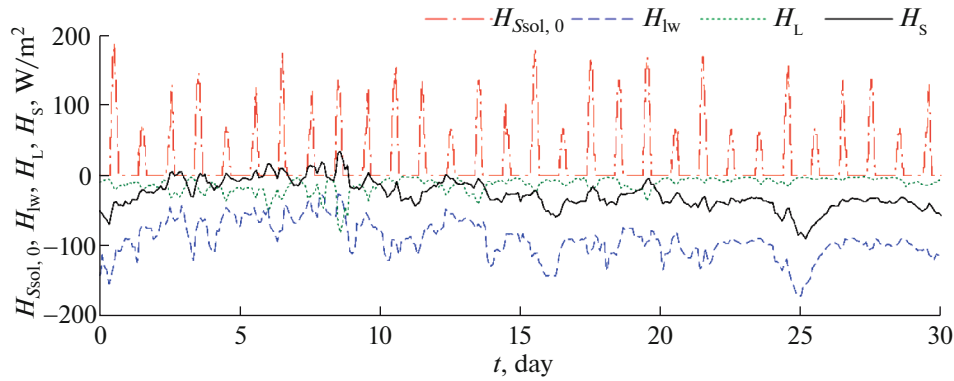
Fig. 2. The calculated values of heat fluxes from December 1 through December 30, 2015 (local standard time).
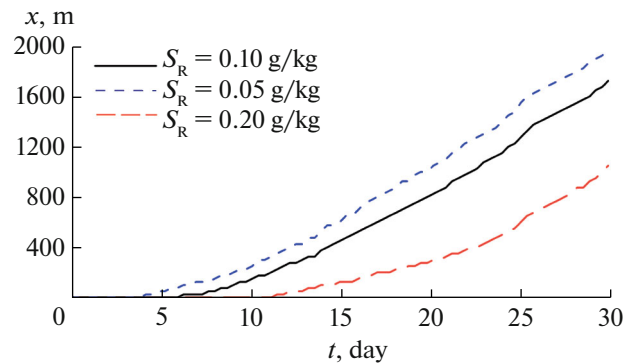
Fig. 3. The dynamics of horizontal movements of the region of the temperature of maximum density at the lake surface.

of values of the sensible heat flux was from 34.1 to -90.1 W/m^2 during the entire month. It is important to note that active long-term cooling of the water surface was observed at nighttime, when there was no solar radiation.

3.2. The River Mineralization Effect on the Evolution of the Thermal Bar

To reveal the effects of mineralization of inflow river waters on the dynamics of the thermal bar, we performed a series of numerical experiments with different values of S_R (Table 1). In experiment 1, the mineralization of the river coincides with that of the lake ($S_R = S_L = 0.1$ g/kg); in experiments 2 and 3, we have $S_R < S_L$ and $S_R > S_L$, respectively.

Table 1. Mineralization of inflow river waters in numerical experiments

Experiment number	S_R, g/kg
1	0.10
2	0.05
3	0.20

Under the condition $S_R = S_L = 0.1$ g/kg (experiment 1), the front of the thermal bar (the line of flow convergence) passes through the region of the temperature of the maximum density ($\sim$4°C), which coincides with its classical interpretation [1, 2]. The thermal bar is formed on the 6th modeling day (Fig. 3, the solid line). On the 20th day, the thermal bar is located at a distance of 750 m from the mouth of the Thompson River (Fig. 4a1). The streamlines indicate that the densest surface waters formed by mixing of warm lake waters ($>$4°C) and cold river waters ($<$4°C) sink in the region of the 4°C isotherm (Figs. 4a1 and 4b1). Sinking waters in the convergence zone lead to the generation of a large vortex in the heat-inert region (to the right of the front of the thermal bar). As the lake is cooled, the thermal bar moves toward the central part of the water body, where its distance reaches 1700 m on the 30th day (Fig. 4b1). The average velocity of the front of the thermal bar at the surface of the lake is 70 m/day. The distributions of isotherms are in qualitative agreement with temperature fields measured at hydrographic stations [21].

In experiments 2 and 3, the region of vortex convergence and the 4°C isotherm do not coincide, which differs from the classical interpretation of a thermal bar. For this reason, below, a thermal bar is under-
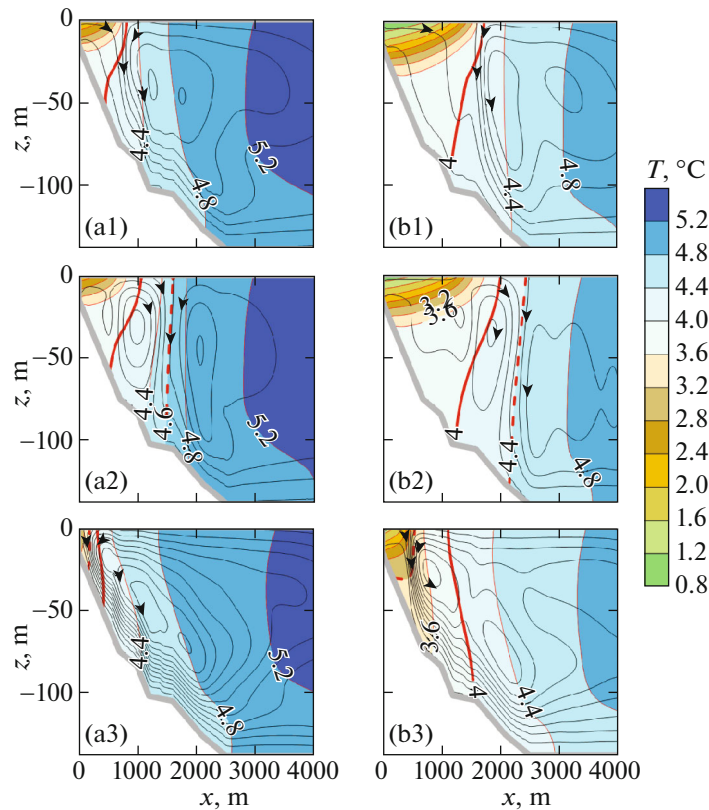
Fig. 4. The isotherms and streamlines for (a) the 20th and (b) the 30th day in numerical experiments with (a1, b1) $S_R = 0.1$ g/kg, (a2, b2) $S_R = 0.05$ g/kg, and (a3, b3) $S_R = 0.2$ g/kg. The solid line shows the 4°C isotherm, while the dotted line shows the isotherm coinciding with the front of the thermal bar.

stood as the line of convergence of the vortex structure.

When river waters are less mineralized (experiment 2), the velocity of the horizontal movement of the thermal bar is higher due to the effects of buoyancy: the less dense (owing to a weaker mineralization) water mass flowing in from the river propagates over the surface of the lake farther (when compared to the results of experiment 1) until it attains the maximum density (Figs. 4a2 and 4b2). In this case, the temperature inside the front of the thermal bar is higher than 4°C: on the 20th modeling day, the temperature in the convergence zone is 4.6°C (Fig. 4a2), and it is 4.4°C on the 30th day (Fig. 4b2). The graph of changes in the location of the temperature of maximum density (Fig. 3, the dotted line) shows that the surface cooling of the lake proceeds faster. It is important to note that there is an intense circulation in the heat-active region (to the left of the front of the thermal bar) in this experiments (unlike experiment 1), and the vortex flow in the heat-inert zone attenuates as the thermal bar moves away from the mouth of the river.

Experiment 3 has shown that when the mineralization of inflow river waters is high, water masses sink along the slope of the bottom and form a large-scale along-slope vortex (Fig. 4a3). The thermal bar evolves

much more slowly (Fig. 4a3 and 4b3). The convergence line passes in the neighborhood of the 3.6°C isotherm (on the 20th day) and the 3.2°C isotherm (on the 30th day). We can conclude from the dynamics of the horizontal movement of the region of the temperature of maximum density (Fig. 3, the dotted line) that the water surface is cooled more slowly in this case than with a low inflow mineralization.

The isohalines also indicate that less-mineralized river waters tend to propagate at the surface of the water reservoir (Figs. 5a2 and 5b2), while saltier water masses intensively sink along the slope under the action of gravity, thus forming a bottom flow (Fig. 5a3 and 5b3).

Thus, numerical modeling has shown that in the period of lake cooling with distinct salinity characteristics of river and lake waters, the zone of convergence of the water masses and the region of the temperature of maximum density cease to coincide, which does not agree with the classical interpretation of a thermal bar as the 4°C isotherm. A similar discrepancy can be also observed with wind loads [23]. In addition, it is worth noting that observations of fronts in estuaries reveal the displacements of the color contrast line and the litter zone with respect to the foam zone, which is a feature of flow convergence at the front [24].
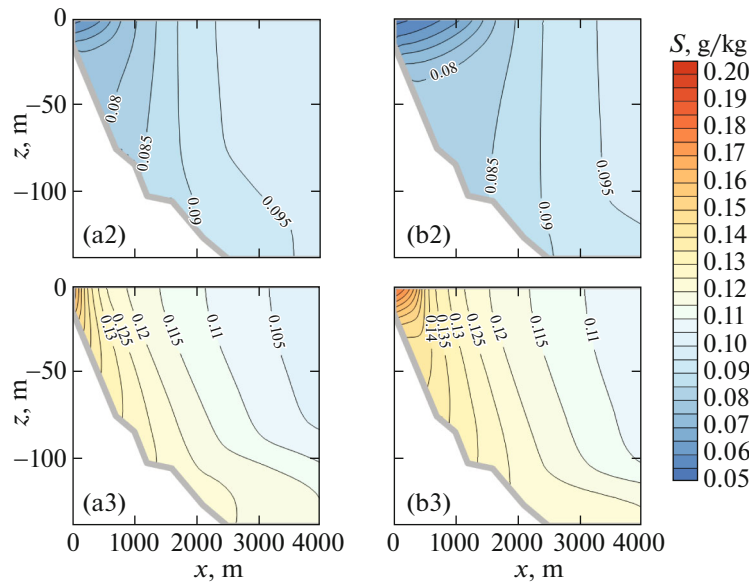
Fig. 5. Isohalines for (a) the 20th and (b) the 30th day in numerical experiments with (a2, b2) $S_R = 0.05$ g/kg and (a3, b3) $S_R = 0.2$ g/kg.

CONCLUSIONS

1. The dynamics of an autumnal river thermal bar were modeled for the first time.

2. The values of the fluxes of short-wave and long-wave radiation and of the latent and sensible heat were calculated for the period of cooling of Kamloops Lake.

3. The distributions of temperature, salinity, and streamlines in Kamloops Lake were obtained for the period of existence of an autumnal thermal bar.

4. Qualitative agreement between calculated temperature fields and data of full-scale observations was obtained.

5. The effect of inflow water mineralization on the evolution of a thermal bar was established.

ACKNOWLEDGMENTS

REFERENCES

1. F. A. Forel, L'Echo Alpes, No. **3**, 149 (1880).

2. A. M. Tikhomirov, *Thermal Conditions in Large Lakes* (Leningrad, 1982).

3. P. R. Holland, A. Kay, and V. Botte, J. Mar. Syst. **43**, 61 (2003).

4. D. E. Farrow and N. R. McDonald, J. Geophys. Res. Oceans **107** (C5), 3033 (2002).

5. N. S. Blokhina, A. E. Ordanovich, and O. S. Savel'eva, Water Resour. **28**, 201 (2001).

6. E. A. Tsvetova, Meteorol. Gidrol., No. 9, 58 (1997).

7. J. Malm, Nord. Hydrol. **26**, 331 (1995).

8. B. O. Tsydenov, A. Kay, and A. V. Starchenko, Proc. Comput. Sci. **51**, 2658 (2015).

9. N. S. Blokhina, Water Resour. **41**, 379 (2014).

10. V. Botte and A. A. Kay, Dyn. Atmos. Oceans **35**, 131 (2002).

11. D. E. Farrow, Environ. Fluid Mech. **2**, 197 (2002).

12. B. O. Tsydenov, A. Kay, and A. V. Starchenko, Ocean Modell. **104**, 73 (2016).

13. M. P. Aleksandrova, S. K. Gulev, and A. V. Sinitsyn, Russ. Meteorol. Hydrol. **32**, 245 (2007).

14. D. C. Wilcox, AIAA J. **26**, 1299 (1988).

15. B. O. Tsydenov and A. V. Starchenko, Vest. Tomsk. Gos. Univ. Mat. Mekh., No. 5, 104 (2014).

16. C. T. Chen and F. G. Millero, Limnol. Oceanogr. **31**, 657 (1986).

17. B. O. Tsydenov, Vychisl. Tekhnol. **22** (S1), 113 (2017).

18. B. O. Tsydenov, Candidate's Dissertation in Mathematics and Physics (Tomsk State Univ., Tomsk, 2013).

19. A. V. Starchenko, Proc. SPIE **9680**, 96800H (2015).

20. I. Orlanski, J. Comput. Phys. **21**, 251 (1976).

21. B. E. St. John, B. C. Carmack, R. J. Daley, et al., *The Limnology of Kamloops Lake, B. C.* (Vancouver, 1976).

22. P. R. Holland, PhD Thesis (Loughborough, 2001).

23. N. S. Blokhina, Moscow Univ. Phys. Bull. **70**, 319 (2015).

24. K. N. Fedorov, *Physical Nature and Structure of Ocean Fronts* (Leningrad, 1983).

Translated by N. A. Berestova